Acta Crystallographica Section D
Biological Crystallography
ISSN 0907-4449

Structure of the Taz2 domain of p300: insights into ligand binding

Maria Miller,[a]* Zbigniew Dauter,[b] Scott Cherry,[c] Joseph E. Tropea[c] and Alexander Wlodawer[a]

[a]Protein Structure Section, Macromolecular Crystallography Laboratory, NCI-Frederick, Frederick, Maryland 21702-1201, USA, [b]Synchrotron Radiation Research Section, Macromolecular Crystallography Laboratory, National Cancer Institute, Argonne, IL 60439, USA, and [c]Protein Purification Core, Macromolecular Crystallography Laboratory, NCI-Frederick, Frederick, Maryland 21702-1201, USA

Correspondence e-mail: mariami@mail.nih.gov

Received 8 September 2009
Accepted 1 October 2009

PDB Reference: Taz2 domain of p300, 3io2, r3io2sf.

CBP and its paralog p300 are histone acetyl transferases that regulate gene expression by interacting with multiple transcription factors *via* specialized domains. The structure of a segment of human p300 protein (residues 1723–1836) corresponding to the extended zinc-binding Taz2 domain has been investigated. The crystal structure was solved by the SAD approach utilizing the anomalous diffraction signal of the bound Zn ions. The structure comprises an atypical helical bundle stabilized by three Zn ions and closely resembles the solution structures determined previously for shorter peptides. Residues 1813–1834 from the current construct form a helical extension of the C-terminal helix and make extensive crystal-contact interactions with the peptide-binding site of Taz2, providing additional insights into the mechanism of the recognition of diverse transactivation domains (TADs) by Taz2. On the basis of these results and molecular modeling, a hypothetical model of the binding of phosphorylated p53 TAD1 to Taz2 has been proposed.

1. Introduction

p300/CBP coactivators link DNA-bound transcription factors (TFs) to the basal transcriptional machinery. Both are large proteins composed of several folded globular domains that are connected by flexible linkers (Dyson & Wright, 2005). Apart from the domains necessary for the acetyltransferase activity, p300 and CBP share highly conserved domains that serve as structural scaffolds for protein ligand binding, including two copies of a zinc-finger domain (Taz1 and Taz2), Kix, Ibid and IHD (Goodman & Smolik, 2000; McManus & Hendzel, 2001). Detailed structural knowledge of these discrete domains and their interactions with transcriptional activators is necessary in order to understand the mechanism of assembly of functional promoter-specific pre-initiation complexes.

The Taz2 domain binds specifically to the acidic transactivation domains (TADs) of several TFs, including the p53 tumor suppressor, ETF2 and members of the STAT and C/EBP families, which exhibit very little sequence similarity. The mechanism of this specific recognition and stimulus-dependent selectivity is poorly understood. Three-dimensional structures have been determined by NMR for unliganded CBP-Taz2 (De Guzman *et al.*, 2000) and its complexes with peptides derived from the TAD of STAT1 (Wojciak *et al.*, 2009) and from the conserved region 1 (CR1) domain of the adenoviral oncoprotein E1A (Ferreon, Martinez-Yamout *et al.*, 2009), as well as for the p300-Taz2–p53-TAD1 complex (Feng *et al.*, 2009). Both STAT1-TAD and p53-TAD1 form short helices upon binding and interact with the Taz2 domain

Table 1
Diffraction data statistics.

Values in parentheses are for the highest resolution shell.

Space group	$I4_132$
Unit-cell parameter (Å)	155.4
Resolution limit (Å)	2.50 (2.59–2.50)
Total reflections	120931 (11805)
Unique reflections	11355 (1108)
Unique Friedel mates	20903 (2091)
Completeness† (%)	100.0 (100.0)
Multiplicity†	5.8 (5.7)
$R_{\rm merge}$†	0.093 (0.647)
$I/\sigma(I)$†	19.2 (2.5)
Wilson B factor (Å^2)	62.8

† Friedel mates treated as separate reflections.

through an extended interface. However, their binding sites overlap only partially and the two polypeptide chains are positioned in opposite directions, with their amphipathic helices occupying distinct sites on the Taz2 surface. In the crystal structure of free Taz2 reported here, the C-terminal helix from a symmetry-generated molecule interacts with the same surface, indicating yet another possible mode of peptide binding to Taz2.

The interaction of CBP/p300 with the TAD of the tumor suppressor protein p53 is of particular interest and has been the focus of intensive studies. It has been shown that p53 interacts with the Taz1, Kix, Ibid and Taz2 domains and probably with the IHD domain (Teufel *et al.*, 2007). The strongest binding of unphosphorylated p53 was observed to the Taz2 domain. The cellular levels and functions of p53 depend on interactions with multiple partners and are regulated by an array of post-transcriptional modifications (for reviews, see Appella & Anderson, 2001; Kruse & Gu, 2009). CBP/p300 competes for binding to the same region of p53 with two negative regulators, MDM2 and MDMX, which are responsible for p53 degradation. Intrinsically disordered p53-TAD is composed of two independent transcriptional subdomains, TAD1 and TAD2, each containing an amphipathic helical motif, $\varphi xx\varphi\varphi$ (where φ denotes a hydrophobic residue), which mediates distinct protein interactions. p53 interacts with MDM2 and MDMX primarily *via* TAD1 (Bottger *et al.*, 1999; Kussie *et al.*, 1996), whereas TAD2 is a major binding site for RPA (Bochkareva *et al.*, 2005) and for the p62 subunit of TFIIH (Di Lello *et al.*, 2006).

The contributions of the two subdomains to Taz2 binding depend on phosphorylation, since p53 is stabilized and activated by phosphorylation of the TAD region in response to DNA damage and other stresses. It has been demonstrated that phosphorylation of Thr18 within p53-TAD1 abrogates its binding to MDM2 and significantly enhances binding to Taz2. The effect of p53 phosphorylation on its binding to Taz2 and MDM2 has previously been investigated by isothermal titration calorimetry, fluorescence anisotropy and NMR spectroscopy (Miller Jenkins *et al.*, 2009; Teufel *et al.*, 2009). However, no satisfactory model for the regulation of p53 activity has emerged from these studies. In particular, structural information on the interaction of Taz2 with the whole TAD of p53 and the structural basis of the increased binding affinity upon phosphorylation of TAD1 at various sites is still lacking. Here, we propose a hypothetical model of p53-TAD1 phosphorylated at Ser15 and Thr18 bound to Taz2 that could reconcile some of the seemingly contradictory published results.

Table 2
Statistics of the refined model of Taz2.

Resolution (Å)	2.50
$R_{\rm work}$	0.206
$R_{\rm free}$	0.236
No. of protein atoms	859
No. of Zn ions	3
No. of sulfate ions	4
No. of waters	31
R.m.s.d. bonds (Å)	0.021
R.m.s.d. angles (°)	2.1

2. Materials and methods

2.1. Protein production and crystallization

Several versions of the Taz2 peptide of varying lengths derived from the human p300 protein were prepared for crystallographic studies: Taz2(1723–1812) and Taz2(1723–1816) correspond to an evolutionarily conserved domain (Yuan & Giordano, 2002), whereas the longer construct Taz2(1723–1836) was designed based on secondary-structure predictions. To prevent misfolding and/or aggregation arising from oxidation, the four Cys residues which are not involved in coordination of the zinc ions (Cys1738, Cys1746, Cys1789 and Cys1790) were mutated to alanines using the QuikChange mutagenesis kit (Stratagene, La Jolla, California, USA). The proteins were expressed in *Escherichia coli* strain BL21-CodonPlus(DE3)-RIL cells (Stratagene) and purified as described previously (Miller Jenkins *et al.*, 2009). The fractions eluted from a Superdex 75 column corresponding to the monomer were collected and concentrated to 2–3 mM. The protein concentration was determined spectrophotometrically and/or using a Bio-Rad assay. The molecular weights of the recombinant proteins were confirmed by electrospray ionization mass spectroscopy and their proper folding was assessed by far-UV CD.

We attempted to grow crystals of the three constructs and their complexes with peptides derived from the p53 TAD. No positive results were obtained on screening for crystallization conditions using vapor diffusion, which was performed with Hydra Plus One and Phoenix robots utilizing a variety of commercial screens or manually in Linbro plates using specially designed conditions with DTT, TCEP or MME being employed as reducing agents. Finally, in order to better prevent oxidation, microbatch crystallization screens were set up manually under paraffin oil in 72-well plasma-treated hydrophilic microbatch plates (Hampton Research). The initial 'hit' was found for the longest peptide, Taz2(1723–1836), using the Precipitant Synergy (Emerald BioSystems) Primary 64 formulations kit. A shower of small crystals appeared when 2.5 M potassium/sodium phosphate buffer pH 7.5 and 20% glycerol (formulation No. 10) were used as the precipitant.

Subsequently, crystallization trials were set up under oil using mixtures of various salts and alcohols. Crystals grew in the pH range 6–7.4 from 1.5–1.7 *M* ammonium sulfate (AMS) solution containing 10–20% glycerol, ethylene glycol or ethanol. No crystals grew when NaCl was used as the precipitant. The best results were obtained when protein at a concentration of 30 mg ml^{-1} in 25 m*M* MES buffer pH 6.3, 100 m*M* NaCl, 6% glycerol, 10 m*M* TCEP was mixed under oil with an equal amount (1 µl) of precipitant containing 3.2 *M* AMS in MES buffer pH 6.0 and 10% ethylene glycol. Crystals grew at 277 K within 2–4 d. The cryoprotectant solution was composed of 1.5 *M* AMS and 25% glycerol. However, the shorter Taz2 peptides failed to crystallize under these or any other conditions.

2.2. Data collection, structure solution and refinement

Diffraction data were collected on SER-CAT beamline 22-ID (APS, Argonne National Laboratory) using a MAR 300 CCD detector. The crystal was cryocooled to 100 K in a stream of cold nitrogen gas. 45 images of 1° oscillation were collected using a wavelength of 1.2827 Å, corresponding to the high-energy remote region of the Zn absorption edge. The data were processed with *HKL*-2000 (Otwinowski & Minor, 1997) and the resulting data statistics are summarized in Table 1.

The structure was solved with *HKL*-3000 (Minor *et al.*, 2006) using the SAD technique based on the anomalous signal of Zn ions present in Taz2. Four fragments of the main chain encompassing 98 residues were built automatically in the initial SAD map. The model of the Taz2 molecule was iteratively completed using *Coot* (Emsley & Cowtan, 2004) and refined with *REFMAC* (Murshudov *et al.*, 1997), with the final model encompassing residues 1726–1834 of the Taz2 sequence. Each long helix of the Taz2 molecule was treated as a separate TLS fragment in the final refinement cycles. The results are presented in Table 2.

Structure analysis and modeling were performed using *Coot* and *INSIGHT* II (Accelrys). Comparisons of three-dimensional models were performed using the *SSM* (*Secondary Structure Matching*; Krissinel & Henrick, 2004) method as implemented in *Coot*.

3. Results and discussion

3.1. Description of the crystal structure

The Taz2 protein (residues 1723–1836) crystallized in space group $I4_132$ with a = 155.4 Å (Table 1). The crystals contained one molecule in the asymmetric unit and the solvent content was quite high at 81%. The packing diagram depicted in Fig. 1

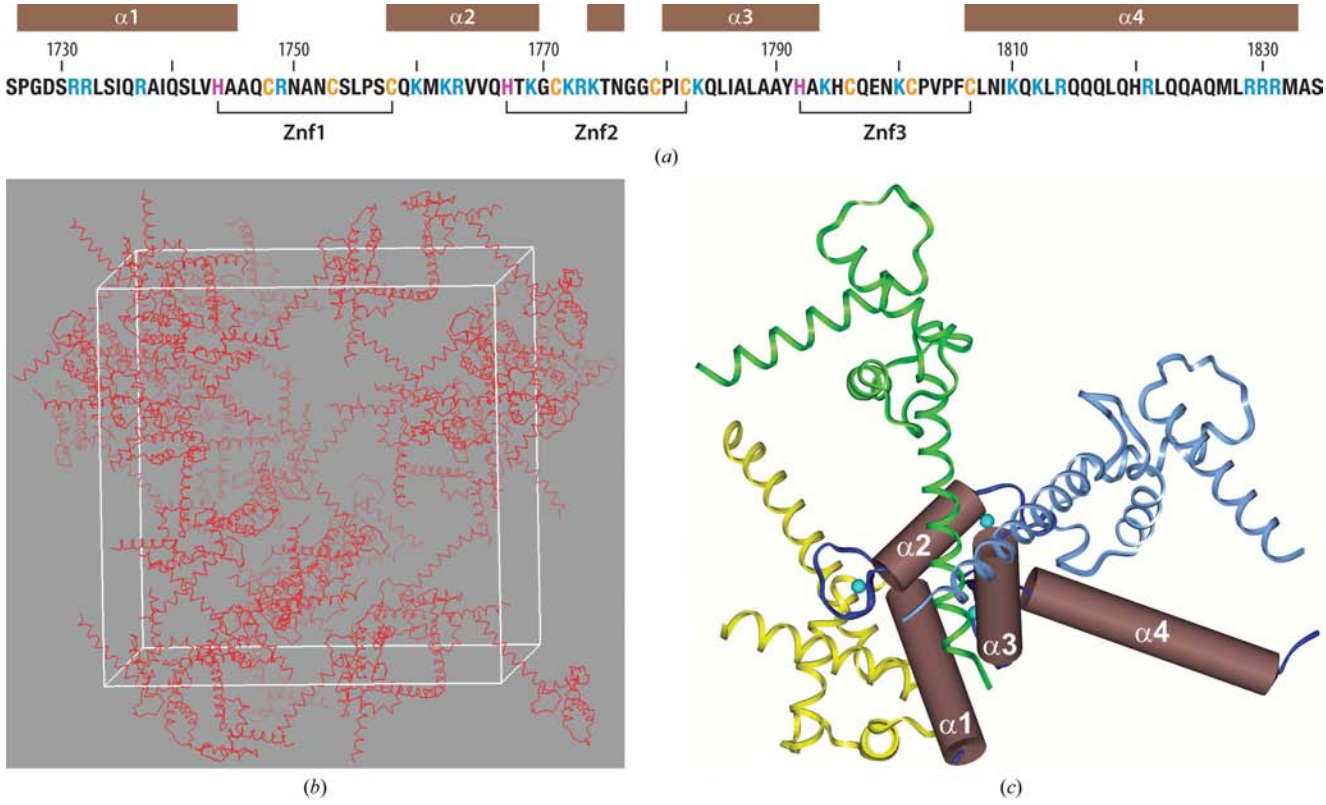

Figure 1
Crystal structure of the Taz2 domain. (*a*) Sequence features of human p300 Taz2 and the secondary structure. Arg and Lys residues are shown in navy blue and Zn^{2+} ligands are highlighted in magenta and orange for His and Cys, respectively. α-Helices are marked by rectangles above the sequence. The zinc-finger subdomains are indicated below the sequence. (*b*) Packing diagram of the 48 molecules contained in the unit cell. (*c*) Taz2 crystallographic model. Helices are represented by brown cylinders, loops are shown in navy blue and Zn ions are depicted as cyan spheres. The molecule of Taz2 forms intimate contacts with three symmetry-generated molecules, which are shown as yellow, gray and green ribbons.

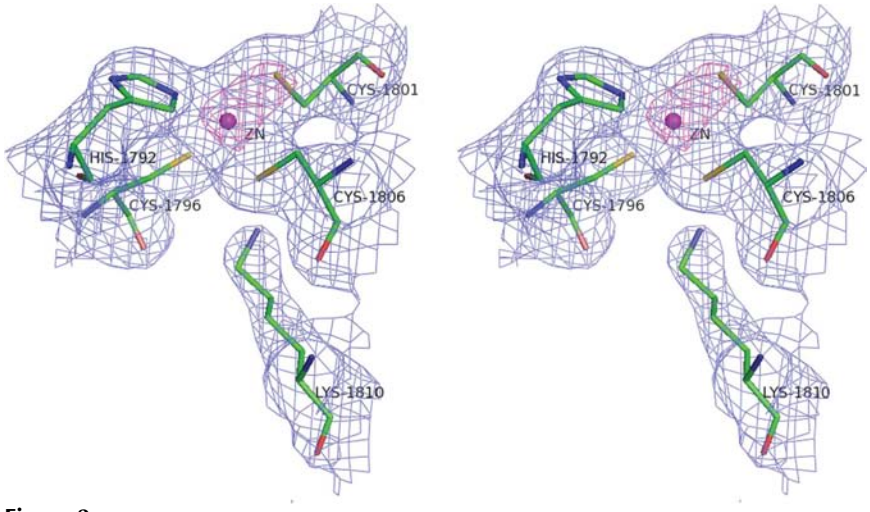

Figure 2
Stereoview of the Znf3 region with the $2F_o - F_c$ electron-density map contoured at 1.8σ (blue) and 8.0σ (magenta).

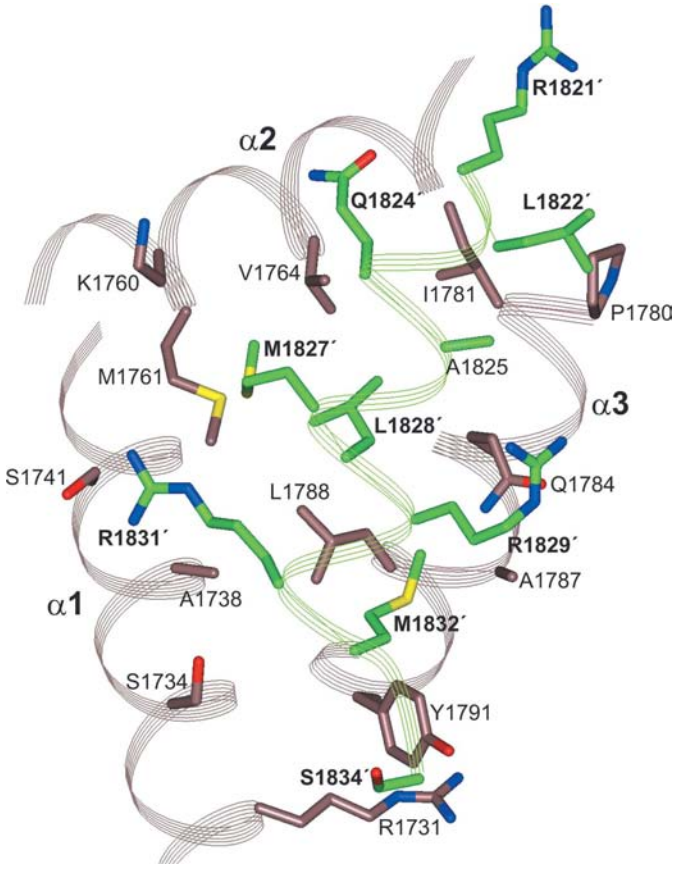

Figure 3
Important crystal contacts: interactions between side chains of Taz2 (chocolate) and the C-terminal part of α4 from a symmetry-related molecule (green). For clarity, side chains that were not involved in intermolecular contacts were omitted.

shows clusters of symmetry-generated molecules and vast solvent channels running parallel to the unit-cell axes. The structure was refined at 2.5 Å resolution to an R factor of 20.6% (R_{free} = 23.6%) with the statistics shown in Table 2. In addition to the protein, the final model included three zinc ions, four sulfate ions and 31 water molecules. The polypeptide chain assumes a compact structure that consists of four α-helices organized by three zinc fingers (Znfs) with HCCC-type coordination (Fig. 1).

It has been established (De Guzman *et al.*, 2000) that the folding of Taz2 into an ordered structure requires the presence of three molar equivalents of Zn ion. Three Zn-binding subdomains are composed of loops linking pairs of helices (α1–α2, α2–α3 and α3–α4) and include the C- and N-termini of consecutive helices (Fig. 1). Each Zn ion is coordinated by a His residue located at the C-terminus of the first helix, two Cys residues from the interhelical loop and a Cys residue located at the N-terminus of the second helix. The requirement for tetrahedral coordination of the Zn ion dictates the crossing angles between helices. The configuration of each zinc finger is stabilized by a set of conserved hydrophobic and electrostatic interactions as described by De Guzman *et al.* (2000). The Zn-coordinating His residues at the C-termini of α1 (His1744), α2 (His1767) and α3 (His1792) contact the side chains of residues from the loops linking the helices (Leu1755, Ile1780 and Val1803), whereas the Cys ligands residing in the loops are stabilized by hydrogen bonds between their S atoms and the backbone NH groups. In the crystal structure, Znf3 is further stabilized by a set of three electrostatic interactions between the positively charged amine group on the side chain of Lys1810 from α4 and (i) the Cys1796 S atom, (ii) the main-chain carbonyl of Cys1796 and (iii) the main-chain carbonyl of Glu1798 (Fig. 2).

The hydrophobic core of the molecule is formed by residues from the three N-terminal helices (α1, α2 and α3) and from the N-terminal part of the fourth helix (α4). 21 residues from the end of α4 protrude outside the globular structure. The helical conformation of this segment is stabilized by a network of electrostatic interactions between polar/charged side chains. Intrahelical links are formed by Gln1816, Lys1812 and Gln1815, by Gln1817 and Arg1821, by Gln1823, His1820 and Gln1824, and by Gln1826 and Arg1830, as well as by the interaction of the Met1827 S atom with the guanidinium group of Arg1831. A continuous hydrophobic patch on the helix surface is generated by the exposed Leu1818, Leu1822, Ala1825, Leu1828 and Met1832, together with the aliphatic portions of the Arg1814 and Arg1821 side chains. This region provides the majority of crystal-contact interactions. The last 14 residues of the molecule generated by the twofold axis (hereafter referred to as α4-end′) make extensive interactions with the residues that maintain the packing of helices α1, α2 and α3 (Fig. 3). The segment Arg1821′–Arg1829′ (where the prime denotes a symmetry mate) interacts with residues from the α2–α3 interface. The interactions are predominantly hydrophobic and include aliphatic portions of the Arg1821′,

Arg1829′ and Gln1824′ side chains. In addition, the guanidinium group of Arg1829′ makes polar contacts with the side-chain carbonyl O atom of Gln1784. Leu1828′ is entirely buried in a deep hydrophobic cavity at the crossing of three helices which is lined by the side chains of Met1761, Val1764, Ile1781, Gln1784, Leu1785 and Leu1788. Met1832′ packs against Ile1735 from α1 and Ala1787, Leu1788 and Tyr1791 from α3. Arg1831′ and Ser1834′ at the C-terminus are bound exclusively by residues from the α1 helix. Ala1738 C^{β} contacts Arg1831′ C^{δ}, while Ser1741 and Ser1734 provide a hydrophilic environment for its guanidinium group. The C-terminal carboxylate and main-chain carbonyl O atoms of Ser1834′ interact electrostatically with the guanidinium group of Arg1731. The loop connecting helices α3 and α4 is also involved in crystal-contact interactions, in which Gln1797 and Glu1798 form a network of hydrogen bonds with Gln1747′, Arg1749′ and Glu1798′ that also involve several water molecules (data not shown). These intimate contacts between molecules in the crystal lattice are facilitated by bound sulfate (SO4) ions. (SO4)204 is tightly bound by the amine groups of Lys1772 and Arg1773, as well as by their backbone NH groups. (SO4)205 interacts with Arg1737 and its symmetry mate, Gln1740, Ser1741′ and Ser1757′. (SO4)206 is located in the vicinity of Arg1829, whereas (SO4)207 bridges Arg1773 and Arg1814′. These contacts explain the requirement for sulfate or phosphate anions for crystallization of the basic Taz2 domain.

3.2. Comparison with the NMR structure of unliganded Taz2

The crystallographic model presented here and the NMR models obtained previously for shorter peptides are very similar (Fig. 4). The NMR-derived structure of free Taz2 superimposes on the X-ray model with an r.m.s.d. of 1.71 Å for 85 common C^{α} atoms. However, the r.m.s.d. was 1.49 Å when only the chains spanning helices α1–α3 were used for superposition. As shown in Fig. 4(*b*), the solvent-accessible residues from the hydrophobic core that stabilize the spatial arrangement of the three helices are mostly unaffected by the crystal-packing forces. In contrast, the inter-helical loop connecting α3 and α4, which is involved in crystal-contact interactions, differs from the solution structure (Fig. 4*c*). Although the segment connecting the two Zn-coordinating Cys residues is in close contact with a twofold axis-related molecule, the configuration of Zn ligands maintaining the tetrahedral coordination of Zn ion is not disturbed.

The α4 helix, which is much longer than its equivalent in the NMR structure of free Taz2, provides additional interactions that contribute to the structural stability of Taz2: Leu1813 makes van der Waals contacts with Ala1793 and Lys1794, and Arg1814 is hydrogen bonded to Asn1799 from the Znf3 region. Comparison of the CD spectra of Taz2(1723–1843) and

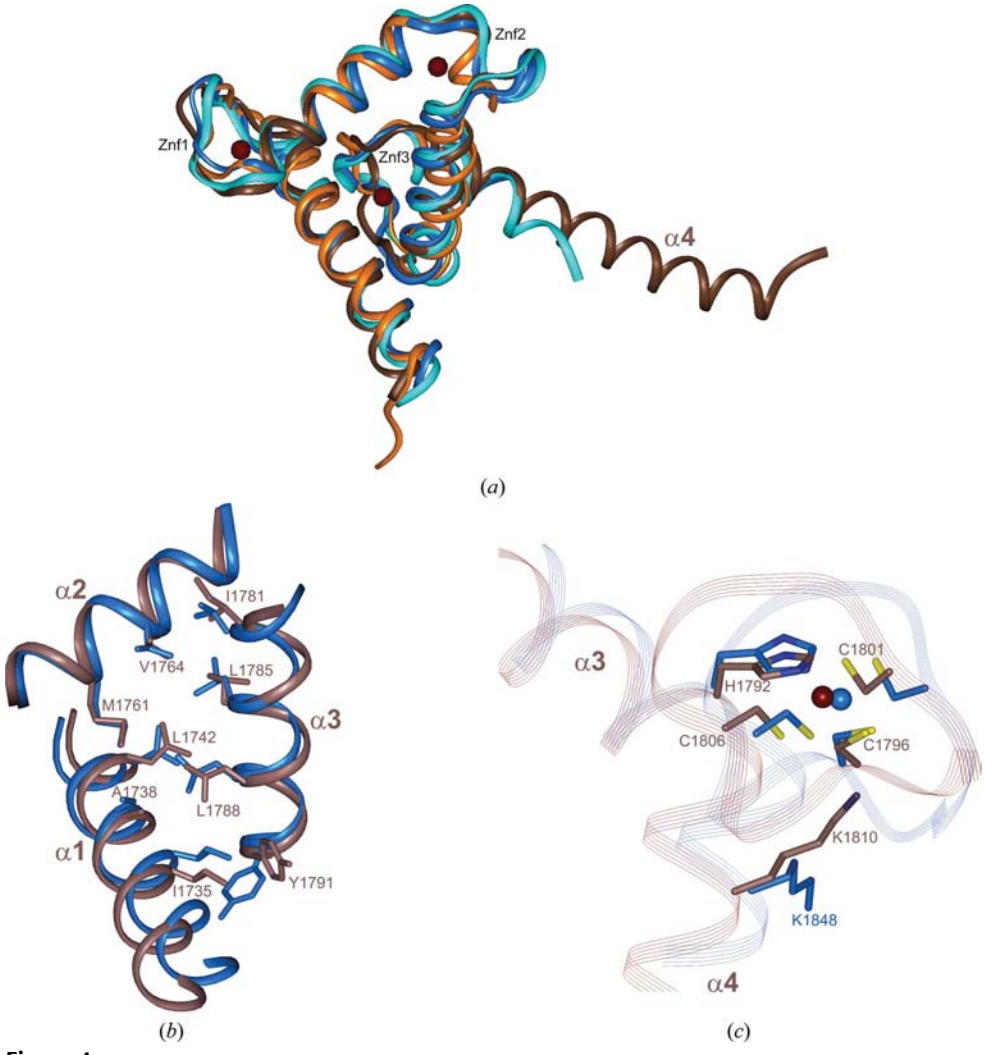

Figure 4
Comparison of crystallographic and NMR models. (*a*) Superposition of the C^{α} traces (shown as ribbons) of the Taz2 crystal structure (chocolate) and the NMR structures of free Taz2 (PDB code 1f81, blue), Taz2 complexed with p53 peptide (PDB code 2k8f, orange) and Taz2 in complex with STAT1 (PDB code 2ka6, cyan). (*b*) Comparison of hydrophobic surfaces of the crystal structure (chocolate) and NMR model (blue) of free Taz2 formed by residues maintaining the packing of helices α1, α2 and α3. The side chains shown are involved in crystal-contact interactions and participate in the binding of the p53 (Feng *et al.*, 2009) and STAT1 (Wojciak *et al.*, 2009) peptides. (*c*) Superposition of the Znf3 regions in the crystal and solution structures. The coloring scheme is the same as above. Protein chains are represented as lines and side chains are shown as sticks, with the S atoms in yellow. Zn ions are shown as spheres. Note the different orientation of p300 Lys1810 and the equivalent Lys1848 in CBP.

the shorter Taz2 protein indicates that this segment retains a helical conformation in solution (see Miller Jenkins *et al.*, 2009).

3.3. Implications forTaz2 ligand binding

The interaction surface for binding of protein ligands revealed by the structures of the Taz2 domain complexed with p53-TAD1 (Feng *et al.*, 2009) and with STAT1-TAD (Wojciak *et al.*, 2009) is shown in Fig. 5. The central hydrophobic area formed by residues maintaining the packing of helices α1, α2 and α3 is flanked by clusters of positively charged residues: Arg1731, Arg1732 and Arg1737 from α1, Lys1760 and Arg1763 from α2 and Lys1772, Arg1773 and Lys1774 from the Znf1 region. The binding site also includes Gln1784, which is an important determinant of binding specificity.

In the crystal structure, the C-terminal end of the α4 helix from a symmetry-related molecule (α4-end′) coincides with the position of the p53-TAD1 helix bound to Taz2. Although the two helices are positioned in opposite directions, Leu22 of p53 and Leu1828′ of Taz2 are buried in the same hydrophobic pocket (Fig. 5*b*). Previous studies (Miller Jenkins *et al.*, 2009) revealed that the peptides representing p53 transcriptional subdomains, TAD1 and TAD2, bind in an anticooperative manner to two overlapping sites on the Taz2 domain. The relatively weak binding of p53-TAD1 to Taz2 is greatly enhanced by the phosphorylation of six possible phospho-acceptors (Ser9, Ser15, Thr18, Ser20, Ser33 and Ser37), with phosphorylation of Ser15 or Thr18 producing the strongest effect. NMR titration showed a sevenfold and 11-fold increase in affinity for Taz2 upon monophosphorylation at Ser15 and Thr18, respectively. Interestingly, only a sevenfold increase was generated upon diphosphorylation at these sites (Feng *et al.*, 2009). Several findings pointed towards the possibility of two distinct modes of interaction with Taz2 for phosphorylated and unphosphorylated forms of p53-TAD1. In the p53-TAD1–Taz2 complex Ser15 is entirely solvent-exposed and mutation of the closest positively charged amino acid, Arg1737, to Ala increased fourfold rather than decreased the binding affinity of p53-TAD1 phosphorylated at this position [p53-(Ser15p)TAD1]. Analogous mutations of Arg1731 or Arg1732, which are proximal to Thr18, decreased the binding affinity of p53-(Thr18p)TAD1 by only twofold. Furthermore, calorimetric as well as chemical shift mapping results for p53-(Thr18p)TAD1 binding indicated changes in the hydrophobic interface of p53-TAD1 with Taz2. Isothermal titration calorimetry experiments showed a significant increase in the contribution of hydrophobic interactions to p53-(Thr18p)TAD1 binding and NMR spectroscopy revealed pronounced differences in the amide chemical shifts of several residues on titration with p53-TAD1 and p53-(Thr18p)TAD (*e.g.* Leu1733, Ile1735 and Ala1738).

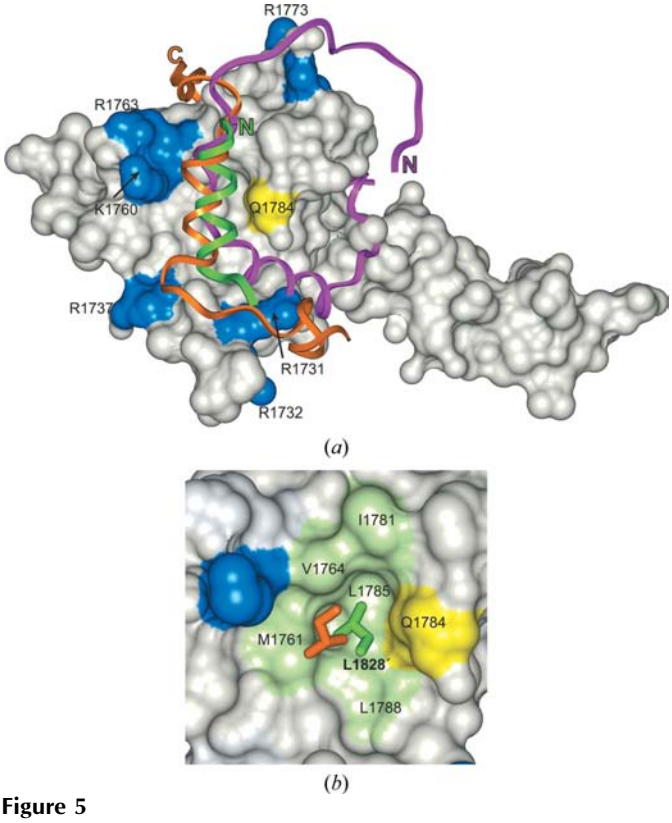

Figure 5
(*a*) Superposition of peptides in the bound conformation (based on structural superposition of Taz2 domains from relevant complexes). The backbones of STAT1, p53-TAD1 and the C-terminus of the symmetry-related molecule in the crystal structure (α4-end′) are rendered as magenta, orange and green ribbons, respectively. The molecular surface of the Taz2 crystal structure is shown in beige, with the Arg side chains in navy blue. Note the reversed directions of the STAT1 and p53 polypeptide chains. (*b*) An enlarged area showing the surface of a hydrophobic cavity (light green) comprised of the side chains of Met1761, Val1764, Ile1781, Leu1785, Leu1788 and the aliphatic portion of Glu1784 (yellow). The side chains of p53 Leu22 from the p53-TAD1–Taz2 complex and Leu1828′ from the α4-end′ are rendered as sticks and shown in orange and green, respectively.

Therefore, we investigated the possibility that a phosphorylated p53 peptide could bind in a manner indicated by the intermolecular interactions in the crystal lattice. As described above, the crystal contacts are mediated by bound sulfate anions and the aliphatic portions of the Arg1821′, Arg1829′ and Gln1824′ side chains make apolar contacts with residues forming the hydrophobic groove on the Taz2 surface. Thus, under crystallization conditions the α4-end′ can mimic an amphipathic helix bound to Taz2. The side chains from the α4-end′ segment were replaced with those from the p53-TAD1 helix (residues 15–26) based on the sequence alignment shown in Fig. 6. The modeling of this interface required only a few adjustments to the Taz2 side chains: Lys1760 was positioned to make a salt bridge with Asp21, Arg1763 was positioned to interact with Thr18 O^{γ} and the aliphatic portions of Lys1783 and Arg1737 were used to complete a hydrophobic environment for Phe19 and Leu25, respectively. Upon *in silico* phosphorylation of Ser15 and Thr18, the side-chain conformations of Lys1760 and Arg1763 were altered to generate the network of electrostatic interactions depicted in Fig. 6. As in the NMR structure of the complex, Phe19, Leu22 and Leu25 provide the most important contributions to the hydrophobic interface, whereas Trp23 is pushed away by the polar amide group of Gln1784, which is partially buried upon complex formation. However, unlike in the unphosphorylated form

Leu26 is also important for binding. This residue is positioned in a hydrophobic pocket created by the side chains of Ile1735, Ala1738, Tyr1791 and Leu1788. These contacts may provide an explanation for the increase in the extent of hydrophobic interactions for p53-(Thr18p)TAD1 compared with the unphosphorylated form, as well as for the observed changes in amide chemical shifts. Also, in this direction of p53 polypeptide binding the phosphorylated Ser9 could potentially interact with Lys1772 and/or Arg1773. Furthermore, p53 Glu28 would be in the vicinity of Arg1731 (Fig. 5*a*), explaining the moderately decreased binding affinity of the Taz2 R1731A mutant protein. On the other hand, mutation of Arg1737 to Ala would remove the unfavorable hydrophilic environment for Leu25 of p53 and should increase the binding affinity, which is in agreement with previous results (Feng *et al.*, 2009).

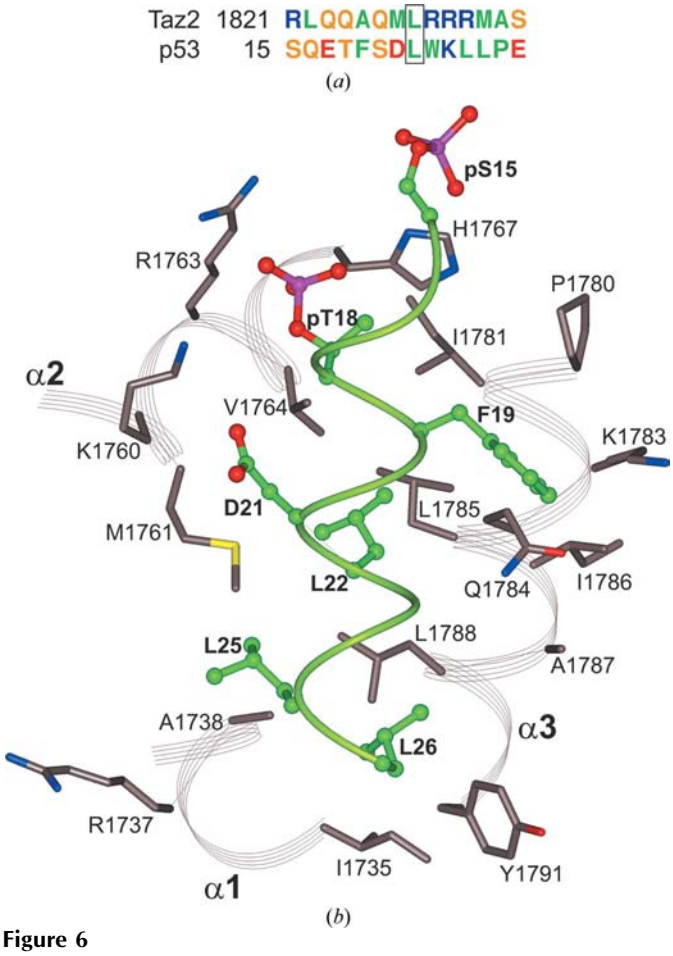

Figure 6
A hypothetical model of a diphosphorylated p53-TAD1–Taz2 complex. (*a*) Sequence alignment of the C-terminal end of Taz2 with the p53-TAD1 peptide used for modeling. Amino acids are colored according to their side chains: hydrophobic, polar uncharged, acidic and basic residues are shown in green, magenta, red and blue text, respectively. Identical residues are boxed. (*b*) Molecular interface of doubly phosphorylated p53-TAD1 (green) with Taz2 (chocolate). For clarity, only the side chains involved in intermolecular contacts are shown. Taz2 side chains are represented as sticks and p53 is shown in ball-and-stick representation. The hydrophobic environment for p53 Phe19, Leu22, Leu25 and Leu26 is provided by Pro1780, Ile1781, Leu1785, the aliphatic portions of Lys1783 and Glu1784, Ile1786, Ala1787, Leu1788 and Tyr1791 from Taz2 α3, and Ile1735, Ala1738 and the aliphatic portion of Arg1737 from α1. The methyl group of Thr18 packs against Ile1781. The complex is stabilized by electrostatic interactions of phosphate groups from pSer15 and pThr18 with Lys1760, Arg1763 and His1767 from Taz2 α2. In addition, there is a possibility of hydrogen-bond formation between p53 Asp21 and Lys1760.

The C-terminus of the α4-end′ overlaps with the N-terminus of the amphipathic helix from the bound STAT1 peptide (Fig. 5), which could indicate the position of binding for the helical binding motif from p53-TAD2. As is the case with STAT1-TAD, this second amphipathic sequence within p53-TAD is preceded by negatively charged amino acids and its affinity of interaction with Taz2 is not affected by phosphorylation (Miller Jenkins *et al.*, 2009). Evidence for overlapping binding sites for p53 TAD1 and TAD2 peptides was provided by ^{1}H–^{15}NHSQC titration experiments on ^{15}N-labeled Taz2 (Feng *et al.*, 2009). Two binding motifs from p53 TAD are separated by a 20-residue flexible linker. According to recent reports (Ferreon, Lee *et al.*, 2009; Teufel *et al.*, 2009), the binding of full-length p53-TAD to Taz2 is dominated by the second motif, with only a minor contribution from TAD1. If this assessment is correct, then only a short helical segment of p53-TAD1 (residues 15–22) would interact with Taz2, whereas Ile1735, Ala1787, Leu1788 and Tyr1791, together with Arg1731 and Arg1732 from α1, would mediate the interactions with TAD2. It is likely that the role of two overlapping sites for p53 binding on the Taz2 surface is to facilitate the formation of multiprotein complexes of varying compositions in response to different stress stimuli and environmental changes. Ternary complexes of MDM2–p53-TAD–CBP/p300 have been observed *in vitro* (Ferreon, Lee *et al.*, 2009) and *in vivo* (Kobet *et al.*, 2000). Ferreon and coworkers demonstrated that unphosphorylated p53-TAD can bind simultaneously to MDM2 through TAD1 and to Taz2 (and also to other CBP domains) through TAD2. The two subdomains behave independently in forming the ternary complex. Phosphorylation of Thr18 abrogates p53 binding to MDM2 and increases its affinity towards CBP/p300. It is therefore conceivable to envision that p53-(Ser15p/Thr18p)TAD1 could be bound to Taz2, whereas TAD2 could interact with another protein partner, with RPA (Bochkareva *et al.*, 2005) and the p62 subunit of TFIIH (Di Lello *et al.*, 2006) being the best candidates of those that have been studied. Further experimental results will be needed to further our understanding of the interactions of p53 with the Taz2 domain of CBP/p300. Whereas determination of the interactions involving the whole p53-TAD may not be feasible, finding the site for p53-TAD2 subdomain binding should be straightforward with the application of the NMR technique.

4. Concluding remarks

We determined the crystal structure of the Taz2 domain of human p300. Comparison with NMR structures confirms that Taz2 is a rigid scaffold for interactions with protein ligands. We observed that the C-terminal helix from a symmetry-related molecule in the crystal lattice interacts with the peptide-binding surface of Taz2, suggesting a putative novel mode of Taz2–peptide ligand interaction. Based on careful analysis of crystal contacts, we examined whether such a mode of inter-

action is possible in the case of p53-TAD1 binding. Modeling indicated that in the absence of TAD2 the isolated unphosphorylated p53-TAD1 peptide may bind to the same site on Taz2 in two alternative orientations. However, upon phosphorylation at Ser15 and/or Thr18 the preferred orientation appears to be determined by electrostatic interactions of the phosphate groups with Lys1760, Arg1763 and possibly Arg1773 of Taz2. The proposed model of phosphorylated p53-TAD1 binding accounts for several experimental results obtained with isothermal titration calorimetry, as well as with NMR spectroscopy, and provides a clue to the mode of interaction of the whole p53-TAD with Taz2.

The polypeptide representing the Taz2 domain used in this study was designed on the basis of secondary-structure predictions and corresponds more to a structural rather than to a functional domain. The resulting structure described here provokes an intriguing question: what is the biological role of the helical C-terminal segment that extends beyond the stable globular structure of Taz2?

We would like to thank Dr Stewart Durell for critical reading of the manuscript. We acknowledge the use of beamline 22-ID of the Southeast Regional Collaborative Access Team (SER-CAT), located at the Advanced Photon Source, Argonne National Laboratory. Use of the APS was supported by the U.S. Department of Energy, Office of Science, Office of Basic Energy Sciences, under Contract No. W-31-109-Eng-38. This project was supported by the Intramural Research Program of the NIH, National Cancer Institute, Center for Cancer Research.

References

Appella, E. & Anderson, C. W. (2001). *Eur. J. Biochem.* **268**, 2764–2772.

Bochkareva, E., Kaustov, L., Ayed, A., Yi, G. S., Lu, Y., Pineda-Lucena, A., Liao, J. C., Okorokov, A. L., Milner, J., Arrowsmith, C. H. & Bochkarev, A. (2005). *Proc. Natl Acad. Sci. USA*, **102**, 15412–15417.

Bottger, V., Bottger, A., Garcia-Echeverria, C., Ramos, Y. F., van der Eb, A. J., Jochemsen, A. G. & Lane, D. P. (1999). *Oncogene*, **18**, 189–199.

De Guzman, R. N., Liu, H. Y., Martinez-Yamout, M., Dyson, H. J. & Wright, P. E. (2000). *J. Mol. Biol.* **303**, 243–253.

Di Lello, P., Jenkins, L. M., Jones, T. N., Nguyen, B. D., Hara, T., Yamaguchi, H., Dikeakos, J. D., Appella, E., Legault, P. & Omichinski, J. G. (2006). *Mol. Cell*, **22**, 731–740.

Dyson, H. J. & Wright, P. E. (2005). *Nature Rev. Mol. Cell Biol.* **6**, 197–208.

Emsley, P. & Cowtan, K. (2004). *Acta Cryst.* D**60**, 2126–2132.

Feng, H., Jenkins, L. M., Durell, S. R., Hayashi, R., Mazur, S. J., Cherry, S., Tropea, J. E., Miller, M., Wlodawer, A., Appella, E. & Bai, Y. (2009). *Structure*, **17**, 202–210.

Ferreon, J. C., Lee, C. W., Arai, M., Martinez-Yamout, M. A., Dyson, H. J. & Wright, P. E. (2009). *Proc. Natl Acad. Sci. USA*, **106**, 6591–6596.

Ferreon, J. C., Martinez-Yamout, M. A., Dyson, H. J. & Wright, P. E. (2009). *Proc. Natl Acad. Sci. USA*, **106**, 13260–13265.

Goodman, R. H. & Smolik, S. (2000). *Genes Dev.* **14**, 1553–1577.

Kobet, E., Zeng, X., Zhu, Y., Keller, D. & Lu, H. (2000). *Proc. Natl Acad. Sci. USA*, **97**, 12547–12552.

Krissinel, E. & Henrick, K. (2004). *Acta Cryst.* D**60**, 2256–2268.

Kruse, J. P. & Gu, W. (2009). *Cell*, **137**, 609–622.

Kussie, P. H., Gorina, S., Marechal, V., Elenbaas, B., Moreau, J., Levine, A. J. & Pavletich, N. P. (1996). *Science*, **274**, 948–953.

McManus, K. J. & Hendzel, M. J. (2001). *Biochem. Cell Biol.* **79**, 253–266.

Miller Jenkins, L. M., Yamaguchi, H., Hayashi, R., Cherry, S., Tropea, J. E., Miller, M., Wlodawer, A., Appella, E. & Mazur, S. J. (2009). *Biochemistry*, **48**, 1244–1255.

Minor, W., Cymborowski, M., Otwinowski, Z. & Chruszcz, M. (2006). *Acta Cryst.* D**62**, 859–866.

Murshudov, G. N., Vagin, A. A. & Dodson, E. J. (1997). *Acta Cryst.* D**53**, 240–255.

Otwinowski, Z. & Minor, W. (1997). *Methods Enzymol.* **276**, 307–326.

Teufel, D. P., Bycroft, M. & Fersht, A. R. (2009). *Oncogene*, **28**, 2112–2118.

Teufel, D. P., Freund, S. M., Bycroft, M. & Fersht, A. R. (2007). *Proc. Natl Acad. Sci. USA*, **104**, 7009–7014.

Wojciak, J. M., Martinez-Yamout, M. A., Dyson, H. J. & Wright, P. E. (2009). *EMBO J.* **28**, 948–958.

Yuan, L. W. & Giordano, A. (2002). *Oncogene*, **21**, 2253–2260.